Huggins, M. L. *J. Chem. Phys.* **1941**, *9*, 440. (c) Huggins, M. L. *Ann. N. Y. Acad. Sci.* **1942**, *43*, 1.
4. Abrams, D.; Prausnitz, J. M. *AIChE. J.* **1975**, *21*, 116.
5. (a) Sanchez, I. C.; Lacombe, R. H. *Nature* **1974**, *252*, 381. (b) Sanchez, I. C.; Lacombe, R. H. *J. Phys. Chem.* **1976**, *80*, 2352. (c) Sanchez, I. C.; Lacombe, R. H. *J. Phys. Chem.* **1976**, *80*, 2568.
6. Kehiaian, H. V.; Grolier, P. E.; Bebson, G. C. *J. Chem. Phys.* **1978**, *75*, 1031.
7. (a) Okada, M.; Nose, T. *Polymer J.* **1981**, *13*, 399. *ibid.* **1981**, *13*, 591.
8. Panayiotou, C.; Vera, J. H. *Polymer J.* **1982**, *14*, 681.
9. Kumar, S. K.; Suter, U. W.; Reid, R. C. *Ind. Eng. Chem. Res.* **1987**, *26*, 2532.
10. Smirnova, N. A.; Victorov, A. I. *Fluid Phase Equilibria* **1987**, *34*, 235.
11. (a) You, S. S.; Yoo, K.-P.; Lee, C. S. *Fluid Phase Equilibria* **1994**, *93*, 193. *ibid.* **1994**, *93*, 215. (c) You, S. S.; Lee, C. S.; Yoo, K.-P. *J. Supercritical Fluids* **1993**, *6*, 69. *ibid.* **1994**, *7*, 251. (d) Shin, M. S.; Yoo, K.-P.; You, S. S.; Lee, C. S. *Int. J. Thermophysics* **1995**, *16*, 723. (e) Yoo, K.-P.; Shin, M. S.; Yoo, S. J.; You, S. S.; Lee, C. S. *Fluid Phase Equilibria* **1995**, *111*, 175. (f) Yoo, K.-P.; Kim, H. Y.; Lee, C. S. *Korean J. Chem. Eng.* **1995**, *12*, 277. *ibid.* **1995**, *12*, 289. (g) Yoo, K.-P.; Kim, J. S.; Kim, H. Y.; You, S. S.; Lee, C. S. *J. Chem. Eng. Japan* **1996**, *29*, 439. (h) Yoo, K.-P.; Lee, C.S. *Fluid Phase Equilibria* **1996**, *117*, 48. Yoo, S. J.; Yoo, K.-P.; Kim, H. Y.; Lee, C. S. *Fluid Phase Equilibria* **1996**, *125*, 21. (I) Yoo, S. J.; Yoo, K.-P.; Lee, C. S. *J. Phys. Chem. B.* **1997**, *101*, 1072.
12. Wilson, G. M. *J. Am. Chem. Soc.* **1964**, *86*, 127.
13. Hill, T. L. *An Introduction to Statistical Mechanics*; Addison Wesley: Massachusetts, 1960; p 296.
14. Timmermans, J. *Physicochemical Constants of Pure Organic Compounds*; Elsevier Scientific Publishing Company: New York, 1950; Vol. 1.
15. Reid, R. C.; Prausnitz, J. M.; Poling, B. E. *The Properties of Gases and Liquids*, 4th eds.; McGraw-Hill Book Co: New York, 1987.
16. Braker, W.; Mossman, A. L. *Matheson Gas Data Book*, 6th ed.; Matheson Gas Products, 1980.
17. van Krevelen, D. W. *Properties of Polymers*; Elsevier Scientific Publshing Company: New York, 1990; Ch. 4-9.
18. Bondi, A. *Physical Properties of Molecular Crystals, Liquids and Glasses*; Wiley: New York, 1986; Ch. 14.
19. Fredenslund, A.; Jones, R. L.; Prausnitz, J. M. *AIChE. J.* **1975**, *21*, 1086.
20. Kac, M.; Uhlenbeck, G. E.; Hemmer, P. C. *J. Math. Phys.* **1963**, *4*, 216.
21. Uhlenbeck, G. E.; Hemmer, P. C.; Kac. M. *J. Math. Phys.* **1964**, *5*, 60.
22. Guggenheim, E. A. *Mol. Phys.* **1965**, *9*, 43. *ibid.* **1965**, *9*, 199.
23. Longuet-Higgins, H. C.; Widom, B. *Mol. Phys.* **1964**, *8*, 549.
24. Beret, S.; Prausnitz, J. M. *Macromolecules* **1975**, *8*, 536.

Oxygen Evolution Reaction at Electrodes of Single Phase Ruthenium Oxides with Perovskite and Pyrochlore Structures**

Eun-Ok Chi, Young-Uk Kwon, and Sun-il Mho*

Department of Chemistry, Sung Kyun Kwan University, Suwon 440-746, Korea
**Department of Chemistry, Ajou University, Suwon 442-749, Korea*
Received May 12, 1997

Single phase ruthenium oxides with perovskite ($ATi_{1-x}Ru_xO_3$ (A=Ca, Sr)) and pyrochlore structure ($Bi_2Ru_2O_7$, $Pb_2Ru_2O_{6.5}$) have been prepared reproducibly by solid state reaction methods and their electrocatalytic activities for oxygen evolution have been examined by Tafel plots. Tafel slopes vary from a low value of 42 mV/decade up to 222 mV/decade at room temperature. The high exchange current densities and high Tafel slopes compared with those obtained from the RuO_2 DSA electrode at the crystalline single phase metal oxide electrodes suggest that they are better electrocatalysts at low overpotentials. A favorable change in the Tafel slope for the oxygen evolution reaction occurs as the ruthenium content increases. Substitution of Ti for Ru in the perovskite solid solutions enhanced their chemical stability by losing marginal electrochemical activity.

Introduction

The oxygen evolution and reduction reactions are of special importance in water electrolyzers, fuel cells, and batteries using air cathodes since slow kinetics of these reactions are the chief cause of efficiency losses.[1] Transition metal oxides possess many of the desirable characteristics for practical electrodes for oxygen evolution.[2] The poor stability of some metal oxides over anodic potential ranges where oxygen evolution takes place is a major problem. Dimensionally stable anode (DSA) materials have been attractive elec-

*To whom correspondence should be addressed
**This article is dedicated to Prof. Woon-kie Paik (Sogang University) in commemoration of his 60th birthday.

trocatalysts for both the chlorine and oxygen evolution reactions.[3] DSA electrodes such as RuO_x are commonly prepared by thermal decomposition of $RuCl_3$ and $Ru(NO)(NO_3)_3$, which are applied as thin coating on metallic substrate, usually titanium.[4-6] Generally, the oxide layers are nonstoichiometric with structural defects. The properties of the oxide layer, especially its catalytic effects depend on the thermal decomposition conditions such as concentration of the salt solution, temperature, atmosphere and duration of heating, and the substrate.[7]

Perovskite-type $CaRuO_3$ and $SrRuO_3$ are metallic conductors. Ru ions in these compounds can be replaced by Ti to form solid solutions $ATi_{1-x}Ru_xO_3$ (A=Ca, Sr) in the whole range of x. The conductivity mechanism changes from metallic to semiconducting as x decreases below 0.5.[8,9] However, we expected that the chemical stability of these Ru compounds can be increased by the Ti substitution. These materials are expected to have a varying electrocatalytic activity and chemical stability depending on their chemical composition. Also, metal oxides with the pyrochlore structure such as $Bi_2Ru_2O_7$ and $Pb_2Ru_2O_{6.5}$, which are all characterized by an infinite, 3-dimensional cubic array of oxide ion as in the perovskite structure, are known to show encouraging performance for air electrodes.[10,11] In the present study, single phase ruthenium oxides with perovskite and pyrochlore structures have been prepared reproducibly by solid state reaction methods and their electrocatalytic activities for oxygen evolution have been examined by Tafel plots.

Experimental

$SrTi_{1-x}Ru_xO_3$ (x=1.0, 0.67, 0.33), $CaTi_{1-x}Ru_xO_3$ (x=1.0, 0.8, 0.6, 0.2, 0) having a perovskite bulk structure, where ruthenium and titanium have an octahedral coordination of 6 oxygens, have been prepared by solid state reactions for electrode materials. The stoichiometric amounts of TiO_2 and $SrCO_3$, and RuO_2 and $SrCO_3$ were mixed and heated at 1100 °C for 20-30 hours in air to prepare $SrTiO_3$ and $SrRuO_3$, respectively. The resulting powders were ground separately, and the mixture of (1-x) $SrTiO_3$ and x $SrRuO_3$ was heated at 1100 °C for 30 hours to synthesize $SrTi_{1-x}Ru_xO_3$ (x=1.0, 0.67, 0.33). $CaTi_{1-x}Ru_xO_3$ (x=1.0, 0.8, 0.6, 0.2, 0) were prepared by a similar procedure at 1300 °C. $Bi_2Ru_2O_7$ and $Pb_2Ru_2O_{6.5}$ have also been prepared by solid state reactions. The stoichiometric amounts of Bi_2O_3 and RuO_2, and PbO and RuO_2 were mixed. The mixture was placed in an alumina boat and sealed in a quartz tube in a vacuum line, which was heated at 700 °C for 15 hrs. and 900 °C for 24 hrs. consecutively for $Bi_2Ru_2O_7$, and at 850 °C for 20 hrs. and at 900 °C for 10 hrs. for $Pb_2Ru_2O_{6.5}$. The structures of the compounds were determined by a Rigaku X-ray powder diffractometer with Cu $K\alpha_1$ radiation.

To make electrodes for the electrochemical measurements, the products were pressed into pellets after mixing the powder with a few drops of binder (4% polyvinyl alcohol solution). The pellets were dried and heated at 1400 °C. One face of the disk was ground with SiC based emery papers (grit #1200, 1500) and polished with alumina (stepwise 1.0, 0.3, 0.05 μm), sonicated and washed thoroughly before use. For comparison, the RuO_2 DSA electrode was prepared by a common technique, *i.e.*, thermal decomposition of a metal salt, $RuCl_3$, on Ti wire.[5]

Table 1. Lattice parameters of the single phase ruthenium oxides with perovskite and pyrochlore structure

	Lattice type	Cell parameter (Å)
$SrRuO_3$	cubic	a=3.932(2)
$SrTi_{1/3}Ru_{2/3}O_3$	cubic	a=3.929(1)
$SrTi_{2/3}Ru_{1/3}O_3$	cubic	a=3.916(2)
$CaRuO_3$	orthorhombic	a=5.533(3), b=5.380(3), c=7.644(5)
$CaTi_{0.2}Ru_{0.8}O_3$	orthorhombic	a=5.531(4), b=5.364(3), c=7.673(5)
$CaTi_{0.4}Ru_{0.6}O_3$	orthorhombic	a=5.530(5), b=5.356(5), c=7.672(4)
$Bi_2Ru_2O_7$	cubic	a=10.315(1)
$Pb_2Ru_2O_{6.5}$	cubic	a=10.267(4)

All electrochemical measurements were made by a Princeton Applied Research Model 263 potentiostat/galvanostat. A three electrode cell system was used: the metal oxide electrode as a working electrode, a platinum wire spiral counter electrode, and a saturated calomel reference electrode (SCE). All potentials reported here are referred to the SCE. The electrolyte was 1.0 M KOH in distilled deionized water. For the Tafel plot, the equilibrium potentials were measured with applying constant currents by chronopotentiometry.

Results and Discussion

The lattice parameters of the compounds of present study are listed in Table 1. While the compounds in the $SrTi_{1-x}Ru_xO_3$ solid solution crystallize in an ideal cubic perovskite structure, the Ca-analogues show orthorhombic distortions. The unit cell parameters decrease gradually with the increase in Ti content in both cases. The pyrochlore compounds show the same lattice parameters as those in the literature indicating that their compositions are close to the ideal ones, *i.e.*, $Bi_2Ru_2O_7$ and $Pb_2Ru_2O_{6.5}$.

A plot of log i (current) *vs.* η (overpotential), known as a Tafel plot, is a useful device for evaluating kinetic parameters.[12] For an anodic branch, the anodic current shows a relationship to the overpotential:

$$i=i_o \exp[(1-\alpha)nF\eta/RT]$$
$$\text{or } \eta=[2.3RT/(1-\alpha)nF] (\log i - \log i_o)$$

where n, F, R, and T are number of electrons, Faraday con-

Table 2. Values of the slopes and exchange current densities from Tafel plots for oxygen evolution in 1.0 N KOH solution at various metal oxides

Metal oxide electrodes		Slope (V/decade)	Exchange current density (A/cm^2)
perovskite structure	$SrTi_{1/3}Ru_{2/3}O_3$	0.096	1.49×10^{-7}
	$SrTi_{2/3}Ru_{1/3}O_3$	0.161	1.30×10^{-5}
	$CaRuO_3$	0.087	3.40×10^{-5}
	$CaTi_{0.2}Ru_{0.8}O_3$	0.197	6.85×10^{-5}
	$CaTi_{0.4}Ru_{0.6}O_3$	0.202	1.53×10^{-5}
	$CaTi_{0.8}Ru_{0.2}O_3$	0.254	2.82×10^{-5}
pyrochlore structure	$Bi_2Ru_2O_7$	0.075	6.30×10^{-8}
	$Pb_2Ru_2O_{6.5}$	0.152	1.58×10^{-5}
DSA type	RuO_2 on Ti	0.056	1.60×10^{-8}

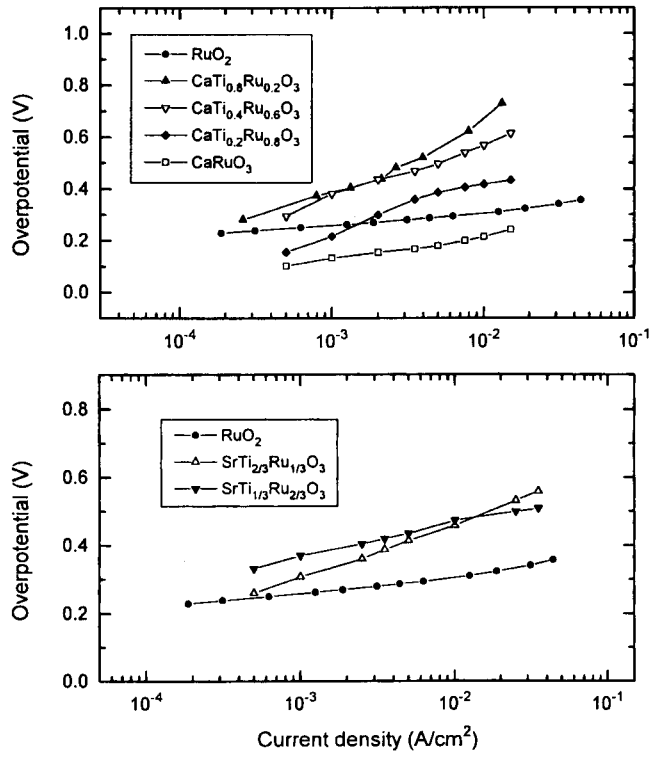

Figure 1. Tafel plots for oxygen evolution in 1.0 N KOH solution at single phase ruthenium oxides with perovskite structure. (a) $CaTi_{1-x}Ru_xO_3$ (x=0, 0.2, 0.6, 0.8, 1.0). (b) $SrTi_{1-x}Ru_xO_3$ (x=2/3, 1/3).

stant, gas constant, and temperature, respectively. The slope of the linear segment is $(1-\alpha)nF/2.3RT$. It extrapolates to an intercept of log i_o. The transfer coefficient α and the exchange current i_o are readily accessible from this kind of presentation. Table 2 summarizes the values of the slopes and exchange current densities from the Tafel plots for oxygen evolution reaction at single phase ruthenium oxide electrodes with perovskite and pyrochlore structures including $SrTi_{1-x}Ru_xO_3$ (x=1.0, 0.67, 0.33) and $CaTi_{1-x}Ru_xO_3$ (x =1.0, 0.8, 0.6, 0.2, 0), and $Bi_2Ru_2O_7$ and $Pb_2Ru_2O_{6.5}$. Tafel plots for oxygen evolution in 1.0 N KOH at various metal oxide electrodes with perovskite structure are also presented in Figure 1. Tafel slopes vary from a low value of 42 mV/decade up to 222 mV/decade at room temperature. A favorable change in the Tafel slope for the oxygen evolution reaction occurs as the ruthenium content is increased, which corresponds to an increase in the transfer coefficient $(1-\alpha)$. $SrTi_{1/3}Ru_{2/3}O_3$ and $CaRuO_3$ and $Bi_2Ru_2O_7$ show lower Tafel slopes (better catalytic effects) for oxygen evolution reaction than the other mixed metal oxide electrodes in this study. The Tafel slopes from our metal oxide electrodes are in the same range as other published works, 30-235 mV/decade.[1] Therefore, the mechanism of oxygen evolution at the metal oxides could be considered to be similar to the previous ones generally accepted[13-15] and that only one electron is involved in the rate determining step at these electrodes. The reaction pathway that is often suggested for oxygen evolution in alkaline solution is as follows[14]:

$$S + OH^- \rightarrow S\text{-}OH + e^- \quad (S \text{ is transition metal ion site})$$

$$SOH + OH^- \rightarrow SO^- + H_2O$$

$$SO^- \rightarrow SO + e^-$$

$$2\,SO \rightarrow 2\,S + O_2$$

The rate determining step (rds) for oxygen evolution of metal oxides varied depending on the electrode material. In addition, the valence states of the cations were found to play an important role in oxygen evolution on metal oxide electrocatalysts. For most cases, one electron process is suggested to be the rate determining step for oxygen evolution processes.[15] From the present study, it was difficult to identify which process is the rds for oxygen evolution at these electrodes. More extensive analysis is required to identify the rds for oxygen evolution.

Table 2 shows that the exchange current densities are in the range from 5.1×10^{-5} to 2.1×10^{-2} A/cm^2. The exchange current density is based on the geometric surface area and the roughness factor is not taken into account. Because of the variability in Tafel slopes obtained from different electrodes, a direct comparison of the exchange current densities as a measure of electrocatalytic activity is not considered to be very useful.[1] For practical purposes, a more meaningful comparison of the electrocatalytic activity of anodes is the overpotential for oxygen evolution that is obtained at a specific current density. $CaRuO_3$ shows the best performance and shows even lower overpotentials than RuO_2 DSA electrode at all current densities (Figure 1a). $CaTi_{0.2}Ru_{0.8}O_3$ shows lower overpotentials at lower current densities and higher overpotentials at higher current densities than the RuO_2 DSA electrode. Higher overpotentials with a large Tafel slope for the oxygen evolution reaction than at the RuO_2 DSA electrode are obtained at oxide electrodes with the lower ruthenium content, $CaTi_{1-x}Ru_xO_3$ (x= 0.2, 0.6). It is well known that in DSA type electrodes (containing RuO_2/TiO_2), the electrocatalytic activity for oxygen evolution decreases dramatically when the ruthenium content is less than 30 mol%.[15] Higher overpotentials for the oxygen evolution reaction than at the RuO_2 DSA electrode are obtained at $SrTi_{1-x}Ru_xO_3$ (x=0.33, 0.67) (Figure 1b). Although $SrTi_{1/3}Ru_{2/3}O_3$ shows lower Tafel slopes for oxygen evolution compared with other oxides in this study, overpotentials are larger at all current densities than the RuO_2 DSA electrode. The $SrRuO_3$ electrode is too unstable in alkaline solutions to make electrochemical measurements. Electrodes of perovskite type $SrTi_{1-x}Ru_xO_3$ (x=1.0, 0.33, 0.67) and $CaTi_{1-x}Ru_xO_3$ (x=1.0, 0.8, 0.6, 0.2) disintegrate during the oxygen evolution reaction in alkaline solutions.

The presence of the mixed valence states of ruthenium in the nonstoichiometric oxides with structural defects, which are prepared by thermal decomposition of metal salts at low temperature (*ca.* 400 °C), is known to correlate with the high electrocatalytic activity. Single phase ruthenium dioxide electrodes of perovskite structures prepared by solid state reaction methods at high temperatures (*ca.* 1200 °C) would have less defects resulting in the valence state of four and a smaller surface area with a crystalline structure. This trend is speculated as the main reason for not showing the expected catalytic effects on the oxygen evolution reaction. In general, the oxygen evolution reaction at the single phase ruthenium oxide electrodes studied in this work results in high exchange current densities and high Tafel

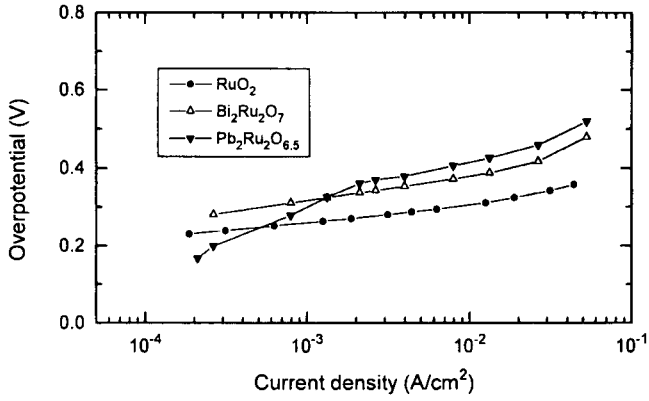

Figure 2. Tafel plots for oxygen evolution in 1.0 N KOH solution at $Bi_2Ru_2O_7$ and $Pb_2Ru_2O_{6.5}$ electrodes of pyrochlore structure.

slopes, compared with the RuO_2 DSA electrode. Therefore, the crystalline single phase metal oxide electrodes appear better electrocatalysts at low overpotentials.

Some oxides with the pyrochlore structure, $A_2B_2O_{7-y}$ (A= Pb, Bi; B=Ru, Ir; $0 \leq y \leq 0.5$), have been found to be active for both oxygen evolution and reduction reactions and are therefore candidate materials for a bifunctional oxygen electrode.[10,11] Oxides with the pyrochlore structure have the ideal chemical formula $A_2B_2O_6O'$; they contain a cubic B_2O_6 framework of corner-shared octahedra that is interpenetrated by an A_2O' subarray. The interpenetrating A_2O' array is flexible, and it may contain O' vacancies. Whereas $Bi_2Ru_2O_7$ has the ideal pyrochlore structure, the Pb analogues contain O'-site vacancies.[16-18] Tafel plots for oxygen evolution in 1.0 N KOH at the electrodes of pyrochlores, $Bi_2Ru_2O_7$ and $Pb_2Ru_2O_{6.5}$, are shown in Figure 2. In the case of $Bi_2Ru_2O_7$, although the overpotentials are larger at all current densities, the Tafel slope for the oxygen evolution reaction is about 60 mV/decade and the linear region in the Tafel plot is comparable to that observed at RuO_2 DSA type electrodes. With $Pb_2Ru_2O_{6.5}$, the slopes for the oxygen evolution reaction are higher than RuO_2 DSA type electrodes. In addition, Tafel slope changes and the linear region in the plot is very limited. The change in the Tafel slope is known to be associated with a change in the valence state or the crystal structure of the metal oxide, *e.g.*, α- or β-$Ni(OH)_2$.[19]

The compounds in the present study and RuO_2 have RuO_6 octahedral units as the building blocks in common but in different modes of connectivity. The octahedra are edge-shared in RuO_2 while they are corner-shared in the others. Since edge-sharing will result in broader d-band through direct d-orbital interactions than in corner-sharing, the mobility of conduction d-electrons will be the highest in RuO_2. Among the structures with corner-shared RuO_2 octahedra, the band width will decrease with the degree of bending in Ru-O-Ru bond angles, which increases along the order, $SrRuO_3$>$CaRuO_3$>$Bi_2Ru_2O_7$>$Pb_2Ru_2O_{6.5}$. However, in the last two pyrochlores $6s^2$-electrons of Bi and Pb would contribute to the conduction electron concentrations to raise their conductivities higher than those of the perovskites. Ti-incorporation into the $ARuO_3$ (A=Ca, Sr) perovskites will localize d-electrons of Ru by creating random potentials and, at the same time, by reducing the d-electron concentration. Therefore, the bulk conductivity of the Ru(IV) compounds will decrease according to the sequence, RuO_2>$Bi_2Ru_2O_7 \geq$ $Pb_2Ru_2O_{6.5}$>$ARuO_3$>$ATi_{1-x}Ru_xO_3$ (A=Ca, Sr). Substitution of Ti for Ru of the perovskite solid solutions causes the loss of electrochemical activity. However, in the case of $SrRuO_3$ electrode, its chemical stability is enhanced by Ti substitution by losing marginal electrochemical activity. Although we have studied only few compositions in this study, more detailed experiments with narrow composition intervals may reveal the optimal composition of acceptable chemical stability and electrochemical activity in these compounds.

Conclusion

Single phase ruthenium oxides with perovskite and pyrochlore structure including $SrTi_{1-x}Ru_xO_3$ (x=1.0, 0.67, 0.33) and $CaTi_{1-x}Ru_xO_3$ (x=1.0, 0.8, 0.6, 0.2, 0), and $Bi_2Ru_2O_7$ and $Pb_2Ru_2O_{6.5}$ have been prepared reproducibly by solid state reaction methods. Their electrocatalytic activities for oxygen evolution have been examined by Tafel plots. The slopes of Tafel plots for oxygen evolution in 1.0 N KOH at various single phase metal oxide electrodes vary from a low value of 42 mV/decade up to 222 mV/decade at room temperature. A favorable change in the slope occurs as the ruthenium content increases, which corresponds to an increase in the transfer coefficient $(1-\alpha)$ for the oxygen evolution. $SrTi_{1/3}Ru_{2/3}O_3$ and $CaRuO_3$ and $Bi_2Ru_2O_7$ show lower Tafel slopes (better catalytic effects) for the oxygen evolution reaction than the other mixed metal oxide electrodes in this study. The bulk conductivity of the ruthenium compounds decreases along the sequence, RuO_2>$Bi_2Ru_2O_7 \geq$ $Pb_2Ru_2O_{6.5}$>$ARuO_3$>$ATi_{1-x}Ru_xO_3$ (A=Ca, Sr). Substitution of Ti for Ru of the perovskite solid solutions causes the loss of electrochemical activity with the enhancement of its chemical stability. Single phase ruthenium dioxide electrodes of perovskite structure prepared by solid state reactions at high temperatures (*ca.* 1200 °C) have less defects, which results in the valence state of four and a smaller surface area with a crystalline structure. This is speculated as the main cause for not showing the expected favorable catalytic effect on oxygen evolution. In general, oxygen evolution reaction at the single phase ruthenium oxide electrodes studied in this work results in high exchange current densities and high Tafel slopes, compared with the RuO_2 DSA electrode. Therefore, the crystalline single phase metal oxide electrodes are suggested to be better electrocatalysts at low overpotentials.

Acknowledgment. This work has been supported in part by the Ministry of Education (BSRI-96-3421) and in part by the Korea Science and Engineering Foundation (96-0501-05-01-3).

References

1. Kinoshita, K. *Electrochemical Oxygen Technology*; Wiley: New York, 1992; and references cited therein.
2. Trasatti, S. *Electrochim. Acta* **1984**, *29*, 1503.
3. Trasatti S.; Lodi, G. in *Electrodes of Conductive Metallic Oxides*; Trasatti, S. Ed.; Elsevier: New York, 1980; Chap. 7 and references cited therein.

4. Yeo, R. S.; Orehotsky, J.; Visscher, W.; Srinivasan, S. *J. Electrochem. Soc.* **1981**, *128*, 1900.
5. Park, S.; Mho, S.; Chi, E.; Kwon, Y.; Yeo, I. *Bull. Korean Chem. Soc.* **1995**, *16*, 82.
6. Ardizzone, S.; Falciola, M.; Trasatti, S. *J. Electrochem. Soc.* **1985**, *136*, 1545.
7. Melsheimer J.; Ziegler, K. *Thin Solid Films* **1988**, *163*, 301.
8. Kobayashi, H.; Nagata, M.; Kanno, R.; Kawamoto, Y. *Mater. Res. Bull.* **1994**, *29*, 1271.
9. Dabrowski, B.; Jorgensen, J.; Minks, D.; Pei, S.; Richards, K.; Vanfleet, H.; Kecker, K. *Physica C* **1989**, *162*, 99.
10. Egdell, R. G.; Goodenough, J. B.; Hamnett, A.; Naish, C. C. *J. Chem. Soc., Faraday Trans.* **1983**, *1*, 79.
11. Gokagac G.; Kennedy, B. J. *J. Electroanal. Chem.* **1993**, *353*, 71.
12. Bard, A. J.; Faulkner, L. R. *Electrochemical Methods*; Wiley: New York, 1980; p 106.
13. Bockris, J. O'M.; Otagawa, T. *J. Electrochem. Soc.* **1984**, *131*, 290.
14. Matsumoto, Y.; Manabe, H.; Sato, E. *J. Electrochem. Soc.* **1980**, *127*, 811.
15. Rasiyah, P.; Tseung, A. C. C. *J. Electrochem. Soc.* **1983**, *130*, 2384.
16. Beyerlein, R. A.; Horowitz, H. S.; Longo, J. M.; Leonowicz, E.; Jorgensen, J. D.; Rotella, F. J. *J. Solid State Chem.* **1984**, *51*, 253.
17. England, W. A.; Cross, M. G.; Mamnett, M.; Wiseman, P. J.; Goodenough, J. B. *Solid State Ionics* **1980**, *1*, 231.
18. Fujishima, A.; Honda, K. *Nature (London)* **1972**, *238*, 37.
19. Gennero de Chialvo, M. R.; Chialvo, A. C. *Electrochim. Acta* **1988**, *33*, 825.

Ligand Field Approach to $4d^1$ Magnetism Based on Intermediate Field Coupling Scheme

Jin-Ho Choy* and Jong-Young Kim

Department of Chemistry and Center for Molecular Catalysis, College of Natural Sciences, Seoul National University, Seoul 151-742, Korea
Received May 16, 1997

The magnetic susceptibilities of molybdenum ions with $4d^1$ electronic configuration in the octahedral crystal field were calculated on the basis of ligand field theory. The experimental magnetic susceptibilities for molybdenum ions, which are stabilized at the octahedral site in the perovskite lattice of $Ba_2ScMo^VO_6$ and $Sr_2YMo^VO_6$, were compared with the theoretical ones. We have tried to fit their temperature dependences of magnetic susceptibility with ligand field parameters, spin-orbit coupling constant ζ_{so}, and orbital reduction parameter κ according to intermediate field coupling and strong field theory. Strong field coupling theory could not explain experimental curves without unrealistically large axial ligand field, since it ignores the mixing up between different state via spin-orbit interaction and ligand field. On the other hand, the intermediate field coupling theory could successfully reproduce experimental data in octahedral and trigonal ligand field. The fitting result demonstrates not only the fact that spin-orbit interaction is primarily responsible for the variation of magnetic behavior but also the fact that effective orbital overlap, enhanced by cubic crystal structure, reduces significantly orbital angular momentum as indicated by κ parameter.

Introduction

In order to interpret the magnetic property of second and third row element, more rigorous calculation is required than the simplified one such as weak field coupling, which has been known to be quite successful in interpreting the magnetic property of first row element. There is a marked difference in the magnetic and optical properties between the $4d^n$ and $5d^n$ transition metal ions and $3d^n$ ones, since spin-orbit interaction as well as ligand field are much stronger than interelectronic repulsion in the former, compared to the latter.[1-7] In fact, in going from $3d$ toward $4d$ and $5d$, we notice that the interelectronic repulsion among the outer shell electrons gets weaker while the spin-orbit interaction becomes stronger. Therefore, the influences of spin-orbit interaction and ligand field need to be relevantly considered. As it is well-known, in the weak field coupling scheme, the starting orbital is d and the zeroth order wavefunctions are

$$|d, m_l=2>,\ |d, 1>,\ |d, 0>,\ |d, -1>,\ \text{and}\ |d, -2>$$

and the zeroth order Hamiltonian consists of the free ion Hamiltonian, given by

$$H_W = H_{core} - \sum_i \frac{Ze^2}{r_i} + \sum_{i \neq j} \frac{e^2}{r_{ij}}$$

where the summation is over all the d electrons. Here H_{core} involves the electrons in the closed shells. The symmetry group of H_W is the full rotation group R_3 in the weak field

*To whom all correspondence should be addressed